Appendix Information for

Single-molecule imaging reveals Tau trapping at nanometer-sized dynamic hot spots near the plasma membrane that persist after microtubule perturbation and cholesterol depletion.

Pranesh Padmanabhan[1,*], Andrew Kneynsberg[1], Esteban Cruz Gonzalez[1], Rumelo Amor[2], Jean-Baptiste Sibarita[3] and Jürgen Götz[1,*]

[1]Clem Jones Centre for Ageing Dementia Research, Queensland Brain Institute, The University of Queensland, Brisbane, Australia 4072

[2]Queensland Brain Institute, The University of Queensland, Brisbane, Australia 4072

[3]Université de Bordeaux, Interdisciplinary Institute for Neuroscience, UMR 5297, Bordeaux, France

[*]**Correspondence:**

Pranesh Padmanabhan or Jürgen Götz

Email: p.padmanabhan@uq.edu.au; j.goetz@uq.edu.au

Appendix Table of Contents

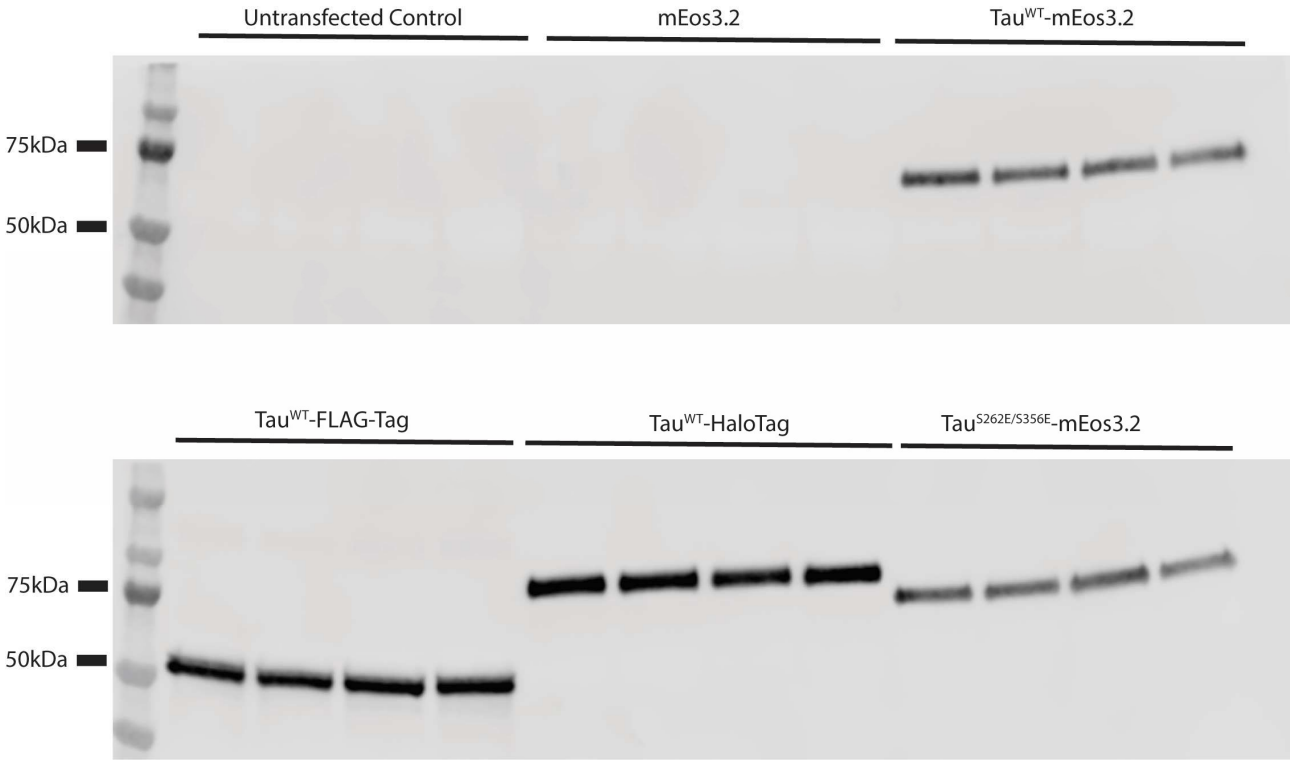

Appendix Figure S1. Western blot analysis of expression of different Tau constructs in N2a cells. Cells transfected with different Tau constructs were analyzed by TAU-5 antibody.

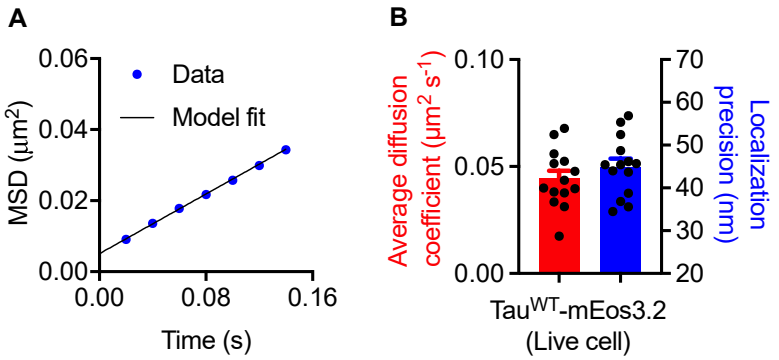

Appendix Figure S2. Estimates of the average diffusion coefficients and the localization precision. A, The average MSD of trajectories from a representative cell was fitted by the equation $MSD(\tau) = 4\sigma^2 + 4D_{avg}\tau$, where D_{avg} is the average diffusion coefficient, τ is the time lag, and σ is the localization precision. **B,** Estimates of D_{avg} and σ from different cells. R^2 was greater than 0.99 for all the fits, and the first four points of the MSD curve were used for fitting (n = 14 live cells).

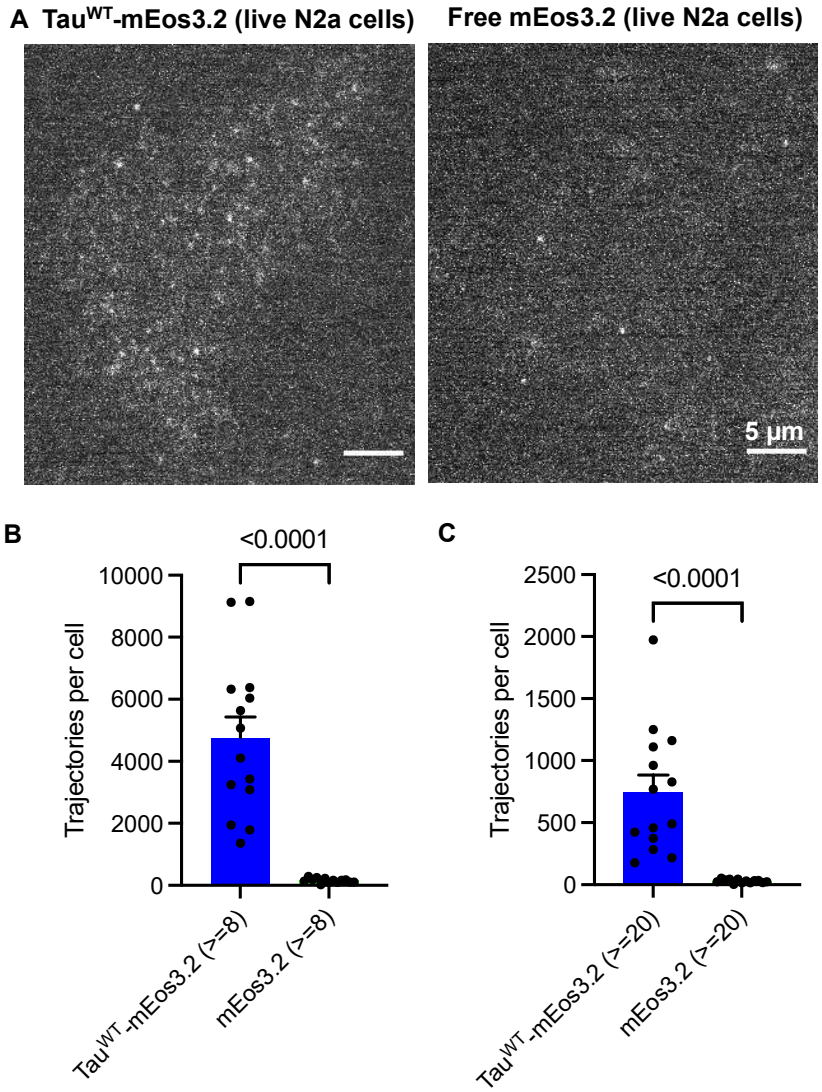

Appendix Figure S3. Statistics of trajectories detected in N2a cells expressing Tau^{WT}-mEos3.2 or free mEos3.2. A, Representative images of live N2a cells expressing either Tau^{WT}-mEos3.2 (left) or free mEos3.2 (right) showing single molecules detected in one frame. **B, C,** Comparison of detected trajectories lasting at least 8 (**B**) and 20 (**C**) frames in live N2a cells expressing either Tau^{WT}-mEos3.2 or free mEos3.2. n = 14 live cells expressing Tau^{WT}-mEos3.2 and 13 live cells expressing free mEos3.2. Statistical analysis was performed using the Student's *t*-test.

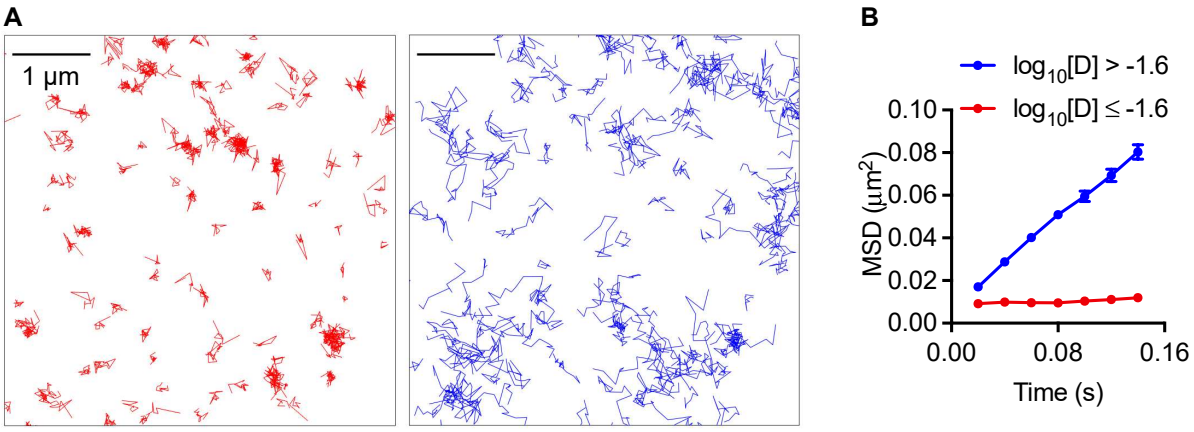

Appendix Figure S4. Tau^{WT}-mEos3.2 trajectories with varying diffusion coefficients in live N2a cells. A, Representative region of a N2a cell with Tau^{WT}-mEos3.2 having $\log_{10}$ [D] ≤ -1.6 (color-coded in red) and $\log_{10}$ [D] > -1.6 (color-coded in blue). **B,** Average mean square displacement as a function of time for trajectories with $\log_{10}$ [D] ≤ -1.6 and $\log_{10}$ [D] > -1.6 (n = 14 live cells).

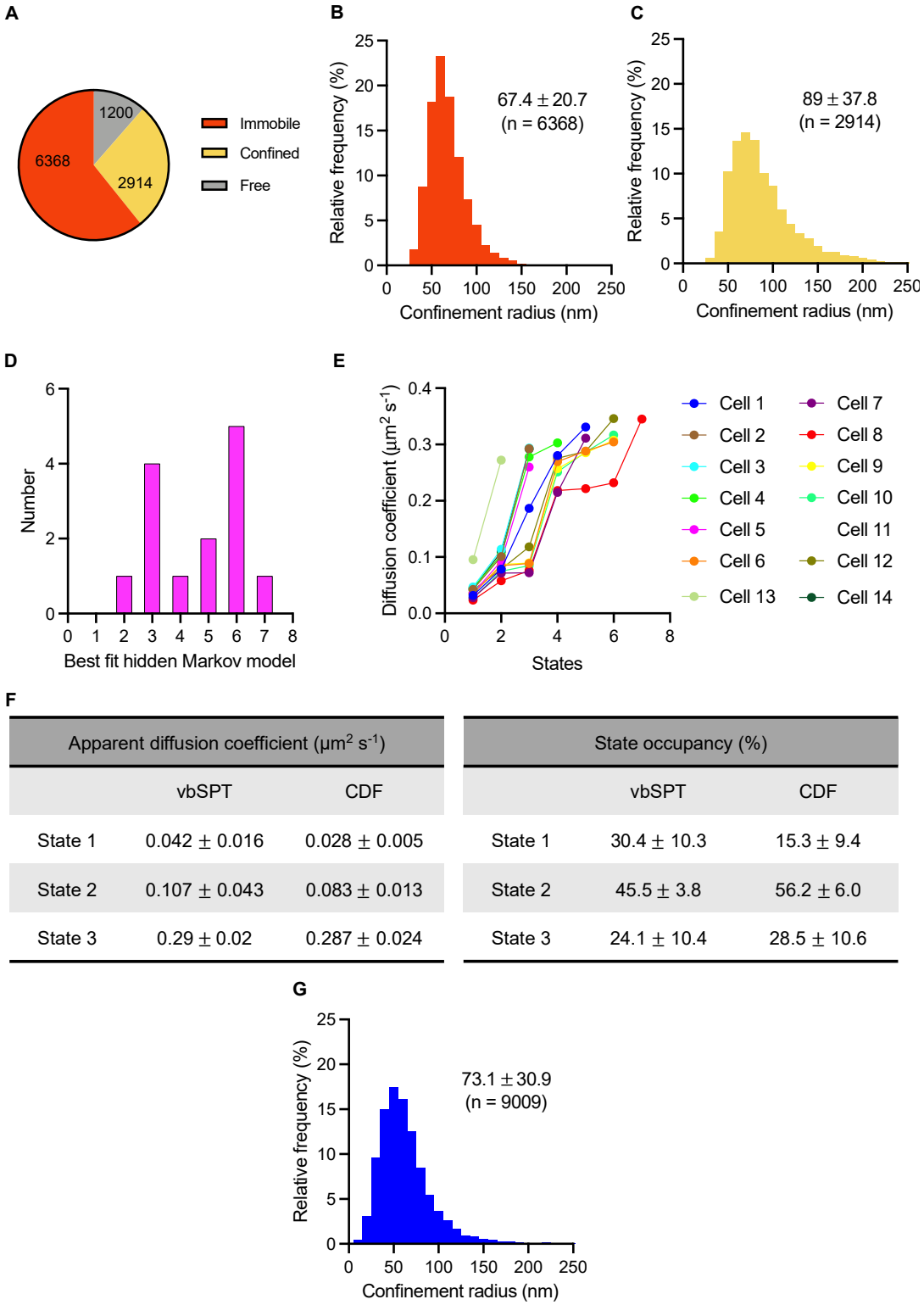

F

Apparent diffusion coefficient (μm² s⁻¹)			State occupancy (%)		
	vbSPT	CDF		vbSPT	CDF
State 1	0.042 ± 0.016	0.028 ± 0.005	State 1	30.4 ± 10.3	15.3 ± 9.4
State 2	0.107 ± 0.043	0.083 ± 0.013	State 2	45.5 ± 3.8	56.2 ± 6.0
State 3	0.29 ± 0.02	0.287 ± 0.024	State 3	24.1 ± 10.4	28.5 ± 10.6

Appendix Figure S5. Detailed analysis of Tau^{WT}-mEos3.2 trajectories. A, The relative distribution of trajectories lasting at least 20 frames annotated as immobile, confined, and diffusive fractions using MSS analysis. **B, C,** The confinement radius of immobile (**B**) and confined (**C**) trajectories identified using MSS analysis. **D,** The distribution of the best fit model by allowing a maximum of 10 hidden states during model selection. **E,** The apparent diffusion coefficients of hidden states of the best fit models. **F,** A summary of diffusion coefficients and state occupancy of a three-state model inferred using hidden Markov modeling (vbSPT tool) and CDF fitting. The mean±s.d. are shown. **G,** The confinement radius of trajectories belonging to hot spots. In **B, C, G,** the confinement radius was computed by eigenvalue decomposition of the variance-covariance matrix of particle coordinates. n = 14 live cells expressing Tau^{WT}-mEos3.2.

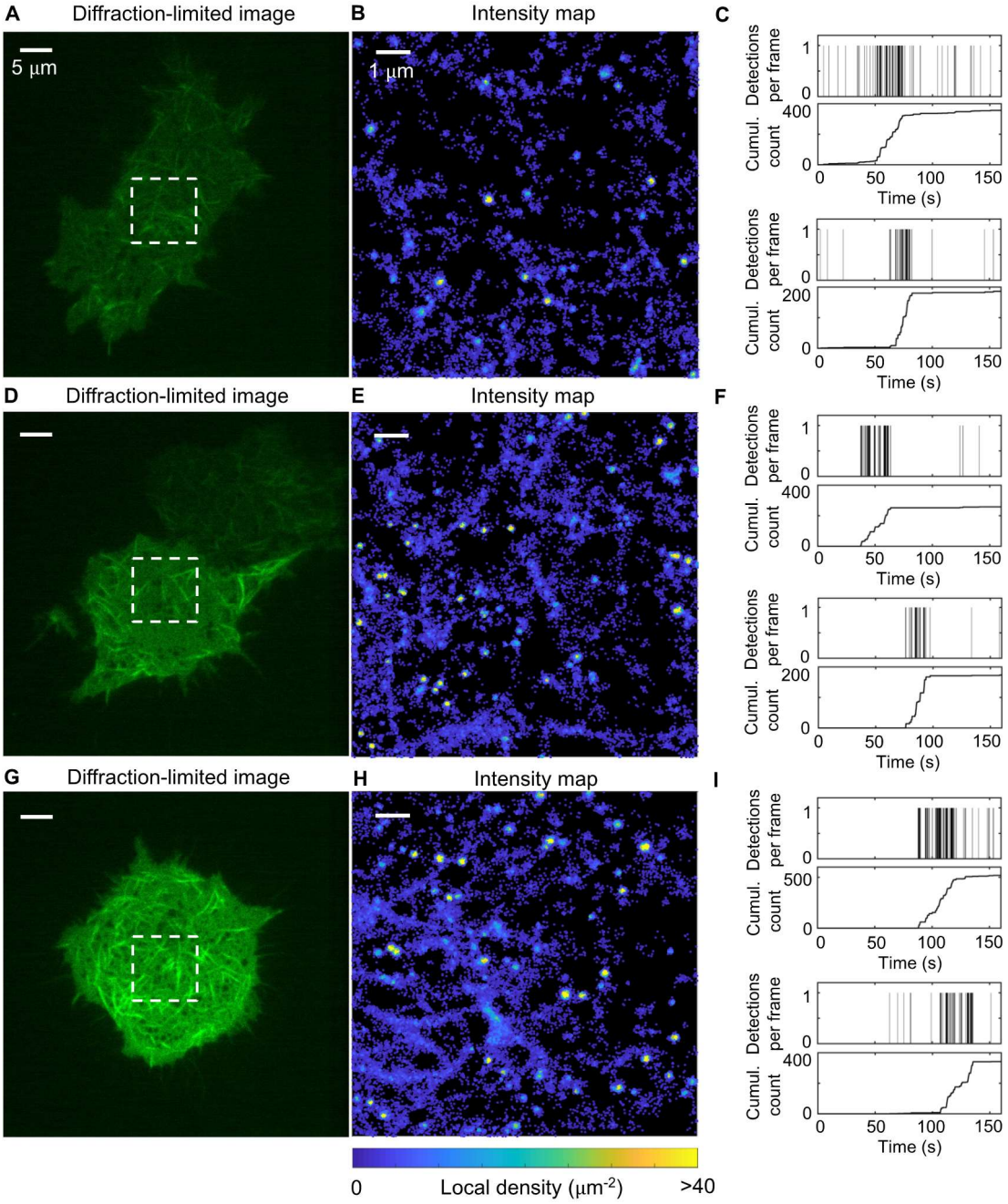

J

Three-state hidden Markov model (vbSPT tool)		
	Apparent diffusion coefficient (µm² s⁻¹)	State occupancy (%)
State 1	0.037 ± 0.009	28.7 ± 10
State 2	0.096 ± 0.017	46.4 ± 7.5
State 3	0.27 ± 0.024	24.9 ± 7.3

Appendix Figure S6. Tau forms hot spots and displays heterogeneous mobility patterns in HEK293T cells. A-I, Representative low-resolution TIRF images (**A, D, G**) and intensity maps (**B, E, H**) of HEK293T cells expressing Tau^{WT}-mEos3.2. Examples of time series of detections from Tau^{WT}-mEos3.2 hot spots detected in these cells (**C, F, I**). **J,** A three-state model was the best fit for all cells (n = 9 live cells) when a maximum of three states was allowed during model selection. A summary of diffusion coefficients and state occupancy of a three-state model inferred using hidden Markov modeling (vbSPT tool). The mean ± s.e.m. is shown.

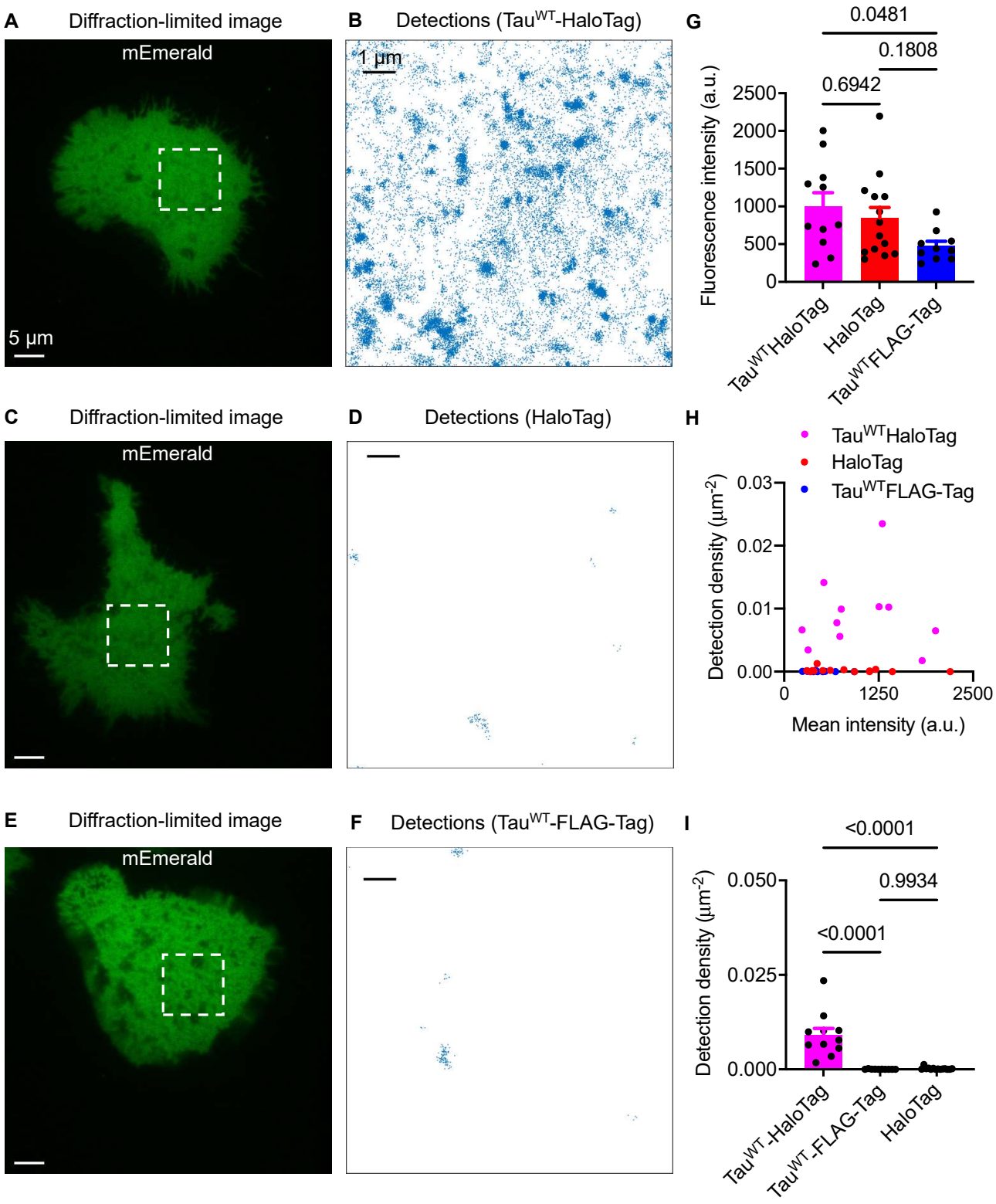

Appendix Figure S7. Statistics of detections in N2a cells co-expressing mEmerald and Tau^{WT}-HaloTag or Tau^{WT}-FLAG-Tag or free HaloTag. A-F, Representative low-resolution TIRF images of mEmerald (**A, C, E**) and maps of detections lasting at least 4 frames (**B, D, F**) of N2a cells co-expressing mEmerald and Tau^{WT}-HaloTag (**A, B**) or free HaloTag (**C, D**) or Tau^{WT}-FLAG-Tag (**E, F**). **G,** Comparison of the intensity of mEmerald across conditions. **H,** Correlation between the detection density and the intensity of mEmerald across conditions. **I,** Comparison of the intensity of mEmerald across conditions. The mean ± s.e.m. is shown. Statistical analysis was performed using one-way ANOVA with Tukey's multiple comparison correction.

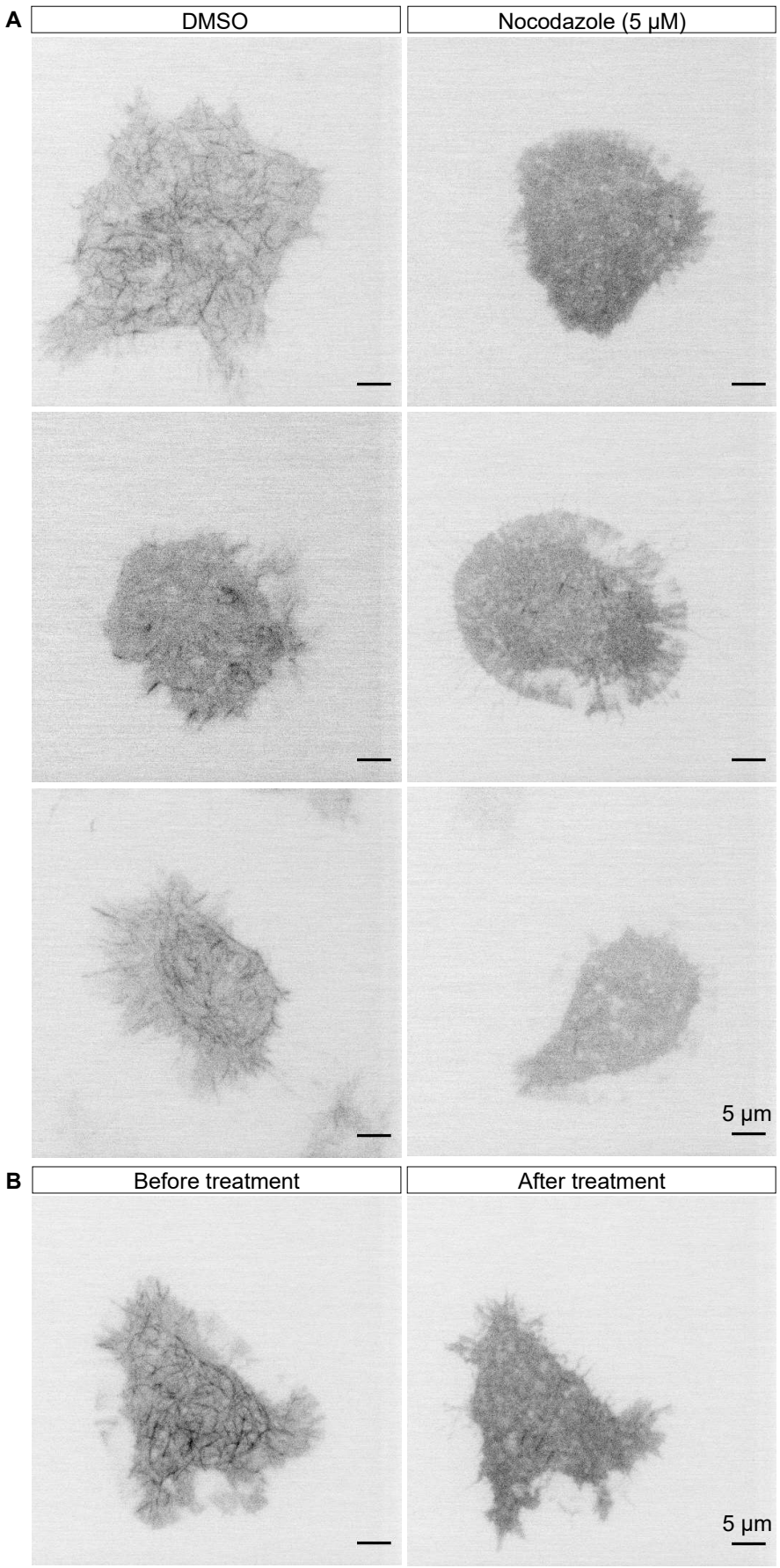

Appendix Figure S8. Nocodazole-treated cells have fewer filament-like structures. A, Low-resolution TIRF images of Tau^{WT}-mEos3.2 in nocodazole-treated (left) and DMSO-treated (right) live cells acquired in the green channel. **B,** Low-resolution TIRF images of Tau^{WT}-mEos3.2 in a live cell before and after nocodazole (5 μM) treatment.

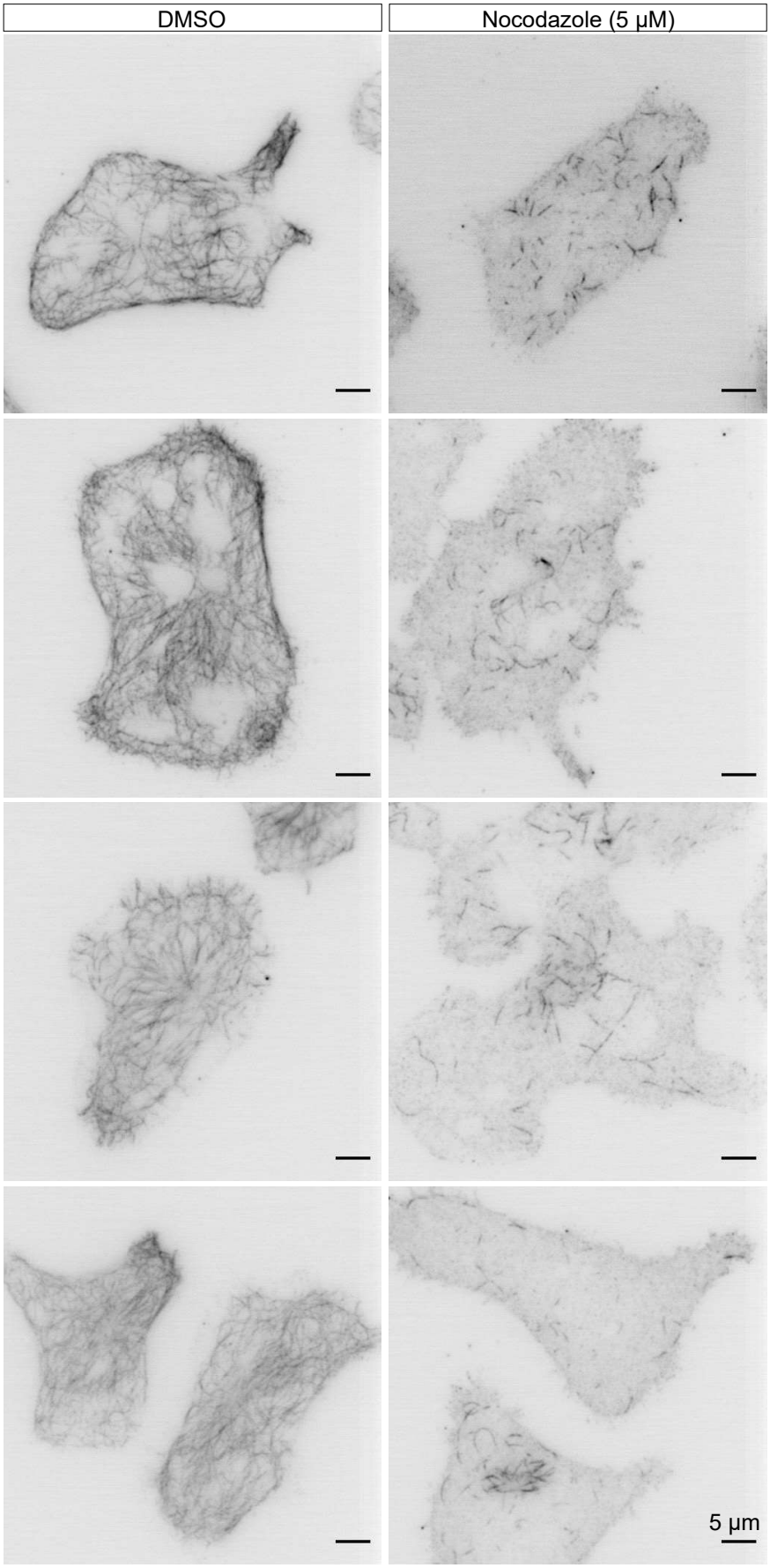

Appendix Figure S9. Nocodazole-treated cells have fewer microtubule filaments. Low-resolution TIRF images of microtubules stained with anti-tubulin antibody in nocodazole-treated (left) and DMSO-treated (right) fixed cells acquired in the green channel.

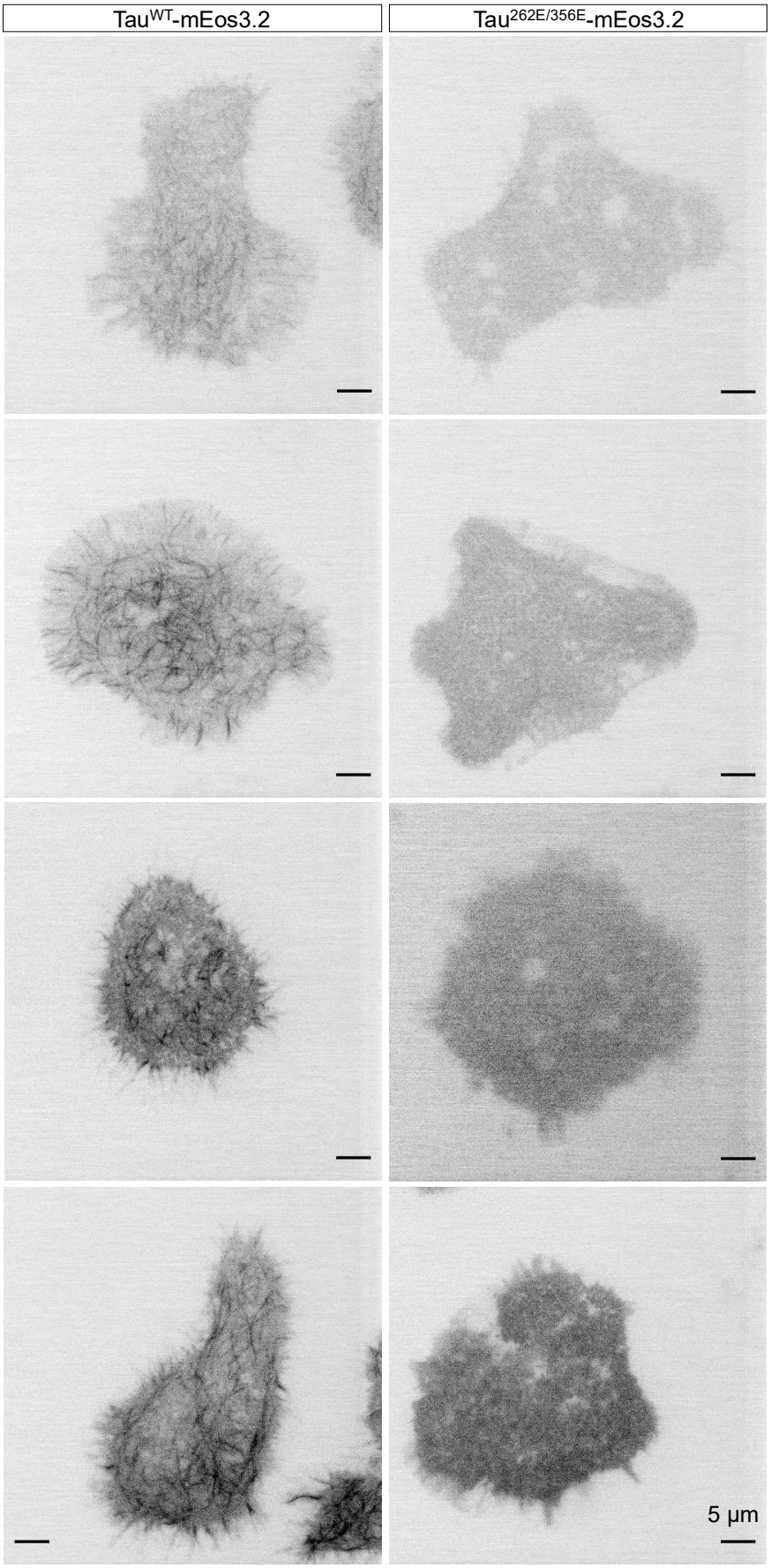

Appendix Figure S10. Microtubule-binding-deficient mutant-expressing cells have fewer filament-like structures. Low-resolution TIRF images of live cells expressing either Tau^{WT}-mEos3.2 (left) or $Tau^{S262E/356E}$-mEos3.2 (right) acquired in the green channel.

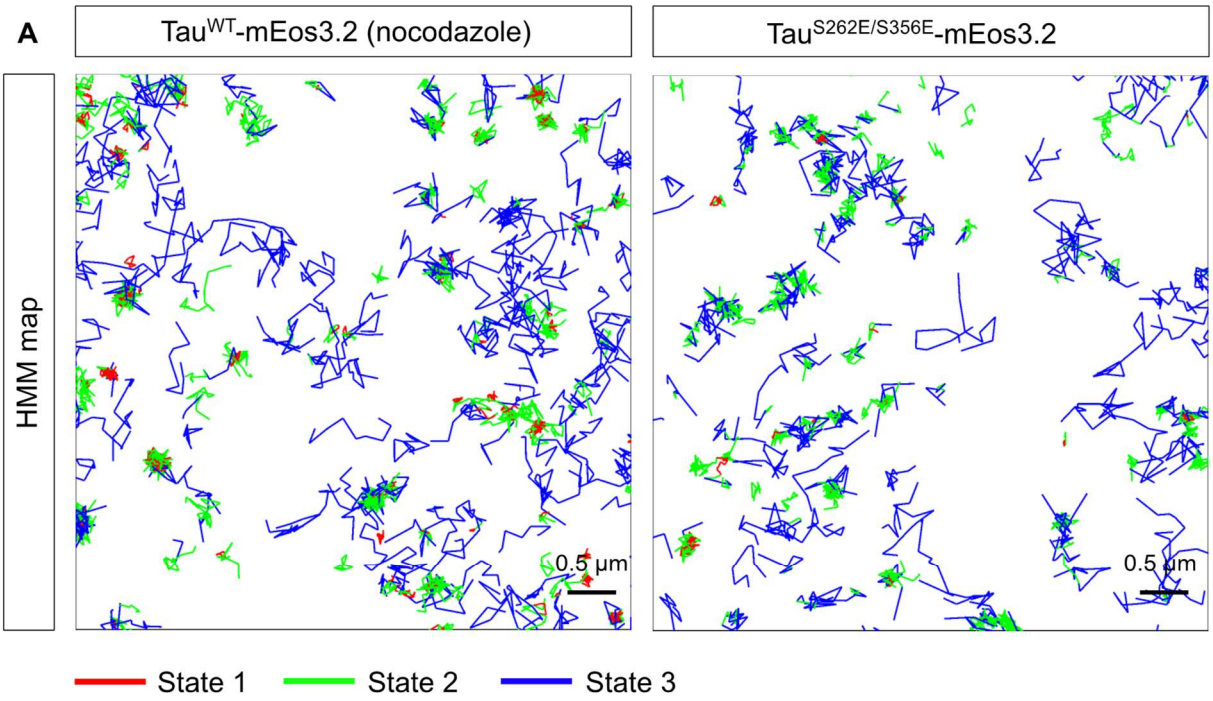

B

Tau^{WT}-mEos3.2 (nocodazole) (n = 29 cells)			Tau$^{S262E/S356E}$-mEos3.2 (n = 39 cells)		
	Apparent diffusion coefficient (μm^2 s^{-1})	State occupancy (%)		Apparent diffusion coefficient (μm^2 s^{-1})	State occupancy (%)
State 1	0.043 ± 0.009	27.9 ± 5.4	State 1	0.061 ± 0.02	28.5 ± 12
State 2	0.116 ± 0.031	41.1 ± 4.0	State 2	0.17 ± 0.07	41.1 ± 5.1
State 3	0.31 ± 0.02	31.0 ± 6.3	State 3	0.33 ± 0.02	30.5 ± 9.8

Appendix Figure S11. Tau displays multiple motion states even after preventing Tau/microtubule interactions. A, Maps of Tau^{WT}-mEos3.2 trajectories in nocodazole-treated cells (left) and Tau$^{S262E/356E}$-mEos3.2 trajectories in untreated cells (right) annotated as distinct diffusive states using the 3-state hidden Markov model. The maps correspond to boxed regions highlighted in Figures 4 and 5. **B,** A summary of the apparent diffusion coefficients and the state occupancies estimated using the 3-state hidden Markov model. The mean ± s.d. is shown.

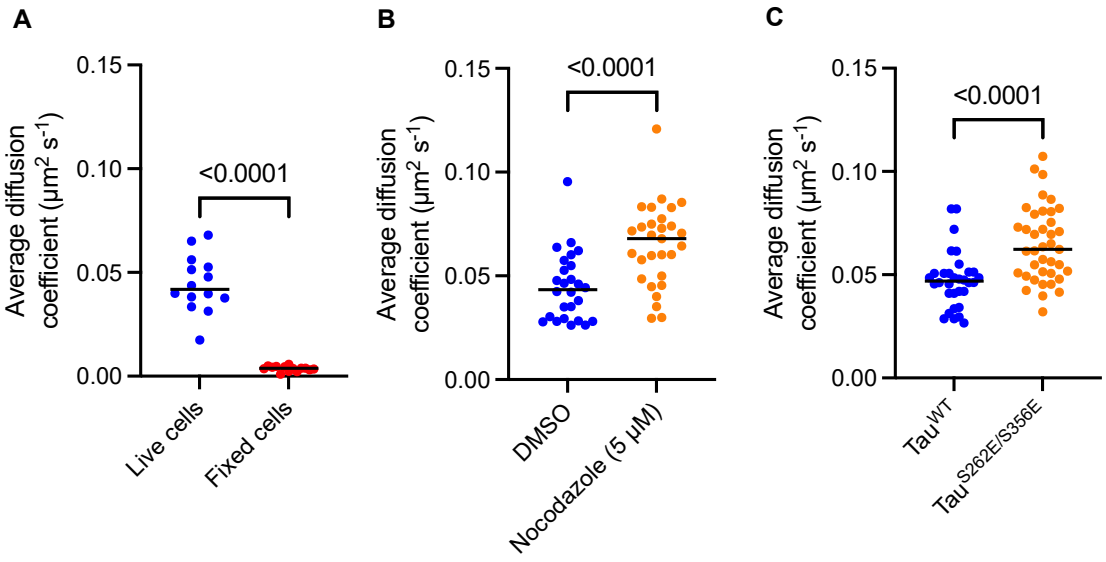

Appendix Figure S12. The average diffusion coefficient of Tau in different conditions. A-C, The average diffusion coefficient of Tau corresponding to data in Fig 1G (**A**), Fig 4E (**B**), and Fig 5F (**C**). Statistical analysis was performed using the Mann-Whitney U test.

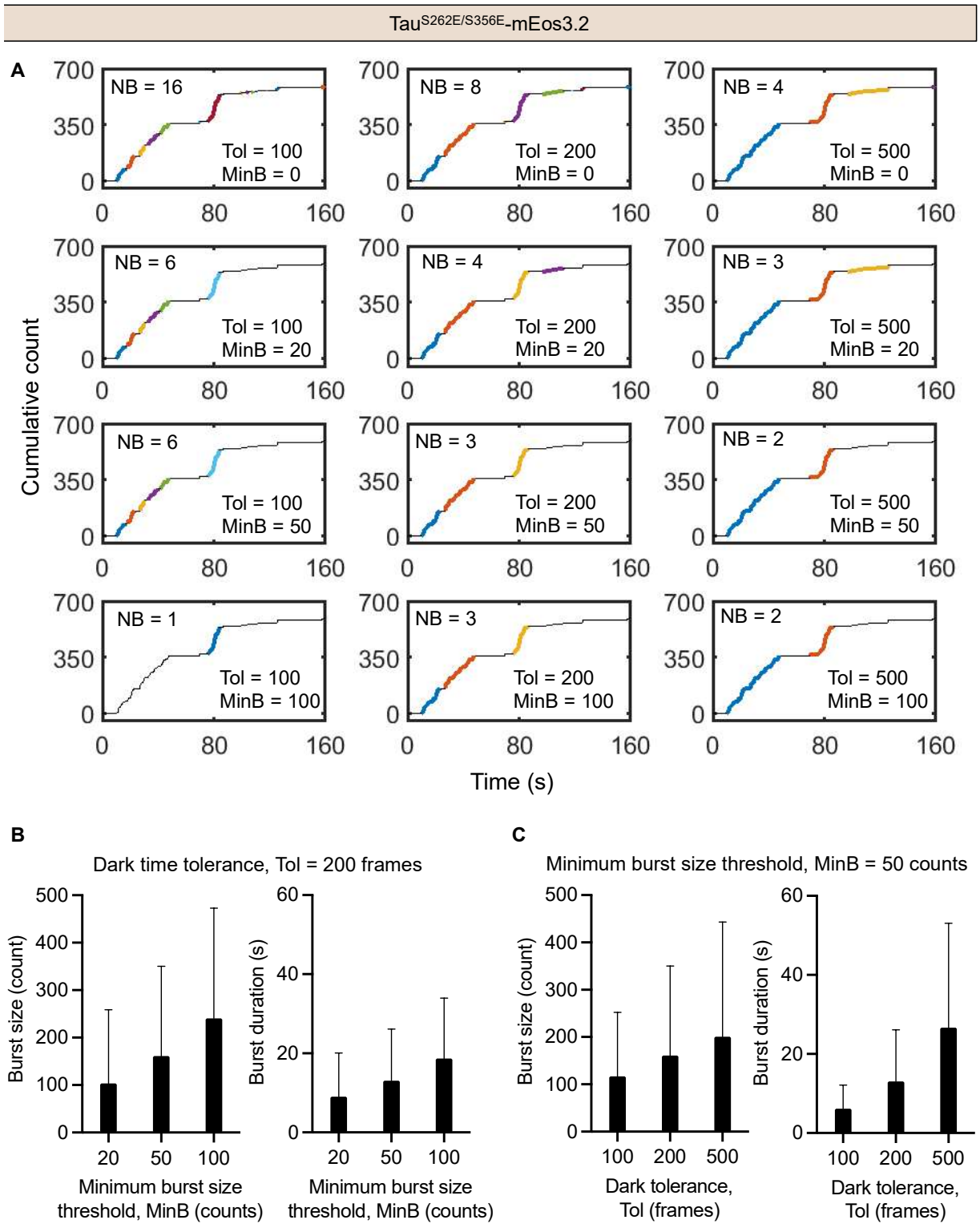

Appendix Figure S13. Sensitivity analysis. A, Representative time series of detections from one Tau$^{S262E/S356E}$-mEos3.2 hot spot. NB is the number of different bursts detected per hot spot (color coded) by varying dark time tolerance, Tol, and minimum burst size, MinB. **B, C,** The burst size and duration as a function of MinB with fixed Tol (**B**) and as a function of Tol with fixed MinB (**C**). The mean ± s.d. is shown in B and C. This analysis corresponds to data in Fig. 6L-N.

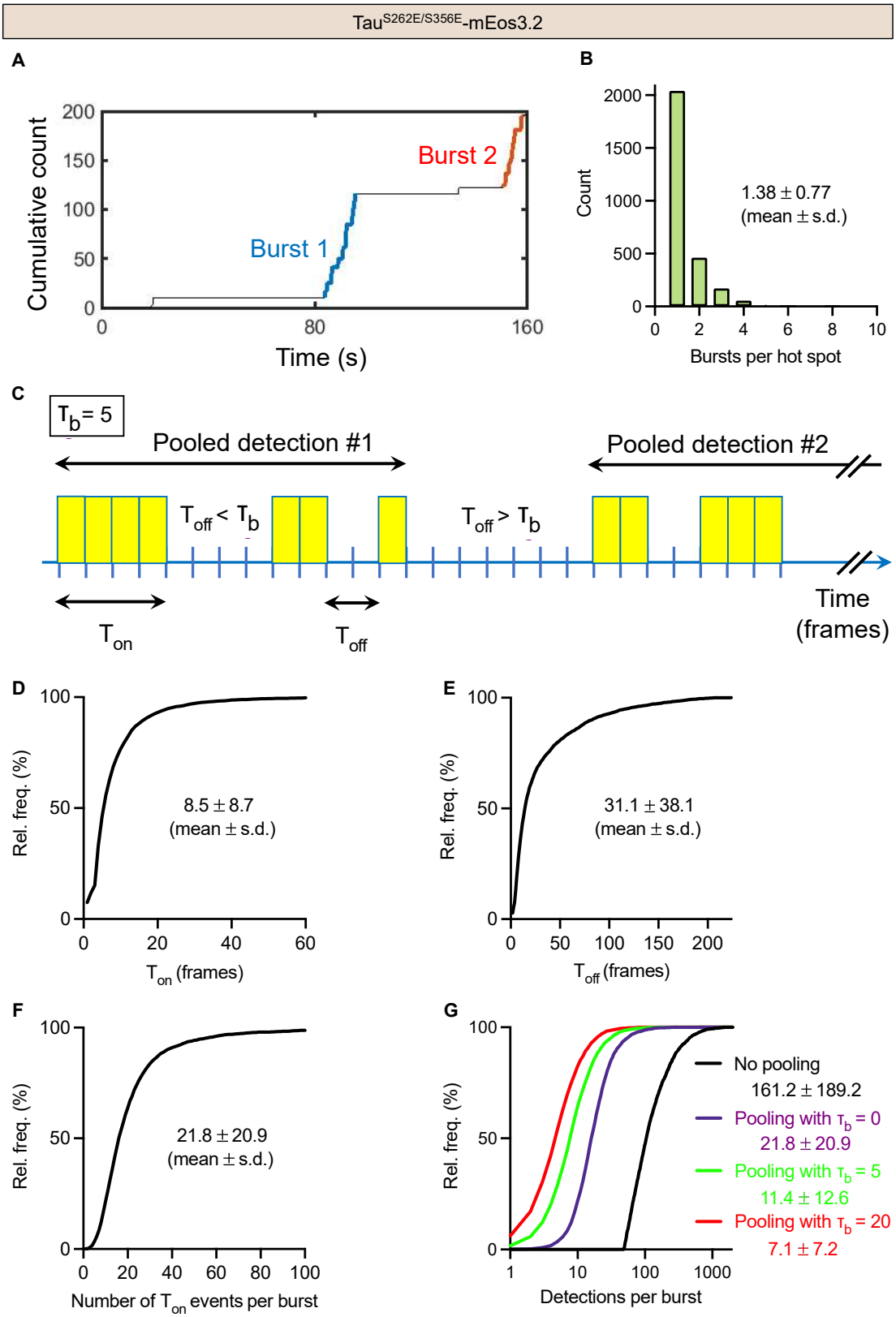

Appendix Figure S14. Sensitivity of burst size to repeated appearances. A, Representative time series of detections from one Tau$^{S262E/S356E}$-mEos3.2 hot spot displaying two bursts. Parameters: Tol = 200 frames and MinB = 50 counts. **B,** The distributions of the number of bursts per Tau$^{S262E/S356E}$-mEos3.2 hot spot. **C,** Schematic of photophysical parameters such as fluorescence on-time, T_{on}, fluorescence off-time, T_{off}, and the blinking tolerance interval, τ_b. **D-F,** The cumulative distributions of T_{on} (**D**), T_{off} (**E**) and the number of T_{on} events per burst (**F**). **G,** The cumulative distribution of the number of pooled detections per burst as a function of blinking tolerance interval, τ_b. This analysis corresponds to data in Fig. 6L-N.